Korean J. Chem. Eng., 33(7), 2240-2251 (2016)
DOI: 10.1007/s11814-016-0046-1

pISSN: 0256-1115
eISSN: 1975-7220

Detection of gas-solid flow faults of a circulating fluidized bed using pressure fluctuations in wind caps

Hua-wei Jiang*,†, Jian-qiang Gao, Hong-wei Chen**, Jun-fu Lu***, Fu-mao Wang****, Yang Wang**, and Zhen-xin Wu****

*Institute of Energy Engineering, Qingdao University, Qingdao 266071, China
**Key Laboratory of Condition Monitoring and Control for Power Plant Equipment of Ministry of Education, North China Electric Power University, Baoding 071003, Hebei Province, China
***Key Laboratory for Thermal Science and Power Engineering of Ministry of Education, Tsinghua University, Haidian District, Beijing 100084, China
****College of Mechanical and Electronic Engineering, Shandong University of Science and Technology, Qingdao 266590, China

(*Received 28 September 2015 • accepted 11 Feburary 2016*)

Abstract−Wind cap partial blockages and agglomeration are two of the most common gas-solid flow faults that occur under the actual operations of circulating fluidized bed boilers. Using the method of measuring pressure fluctuations, for the characterization of fluid dynamics in fluidized beds, has a great advantage, due to its flexible adaptation to any operating conditions to monitor fluidization. This paper presents research into the use of measuring and analyzing pressure fluctuations in wind caps, for the analysis of the gas-solid fluidization characteristics in a fluidized bed with wind cap partial blockages or agglomeration fault. Partial blockages in a wind cap near feeding side and partial blockages in another wind cap near recycling side as well as agglomeration of different extents were simulated in a cold circulating fluidized bed. Pressure fluctuations in the inlets of several wind caps were measured at different primary air velocities under different fault conditions. They were then analyzed with the methods of statistical average, standard deviation, wavelet analysis and homogeneous index. Based on the calculated characteristic parameters, the effects of gas-solid flow faults on the gas-solid fluidization characteristics were analyzed. Results showed that variations of characteristic parameters of pressure fluctuations were related to variations of the gas-solid flow condition, which were caused by wind cap partial blockages or agglomerations. It is shown that the proposed method is practical.

Keywords: Gas-solid Flow, Circulating Fluidized Bed, Wind Cap Partial Blockages, Agglomeration, Pressure Fluctuation

INTRODUCTION

Circulating fluidized bed (CFB) boilers, owing to extensive fuel adaptability and low-cost pollution control, have developed rapidly in recent years and are widely used in power generation by combustion of low grade fuels such as inferior coals, biomass and sewage sludge. Due to complex fuel composition, the combustion process is prone to slagging phenomenon. For example, there is a high content of ash in some coals; during combustion their ash content will react with bed materials, simultaneously generating strong-caking substances, which are able to cause slagging and even agglomeration [1]. There is also a high content of alkali metals in biomass, whose ash fusion point is relatively low, prone to slagging in the furnace [2]. When sewage sludges are mixed with coals for combustion, the large blending combustion proportion of sludges will cause a significant decrease of ash fusion point, with a clear tendency to slagging [3]. Slagging phenomenon will cause abnormal fluidization in furnace, and when severe will result in wind cap blockages and even defluidization.

Wind cap blockage is a kind of common fault taking place in the actual operation of CFB boilers, whose occurrence will also lead to abnormal fluidization in the bed and bring great harm to the safe and economical operation of CFB boilers. Besides slagging in furnace that causes wind cap blockages, under normal operating conditions, those wind caps near recycling inlets, coal injection ports or furnace walls all around are most prone to blockages. Because a large number of materials will be dumped in these areas for fluctuation, whose instant partial pressures may exceed the outlet pressures of the wind caps on the distribution plate, causing recoils of some bed materials into the interiors of caps, and thus result in wind cap partial blockages. It is not hard to see that wind cap partial blockages are associated with large pressure disturbances taking place in beds, and the method using pressure fluctuation signal analysis to predict the occurrence of wind cap partial blockages faults in fluidized beds is feasible.

When an excess temperature of a local bed occurs, due to the defluidization, meanwhile the melting temperature of ash is reached, slagging will appear in the form of agglomerate. The formation of particle agglomeration is one of the most likely phenomena that occur in biomass fired fluidized beds. In the absence of detection,

†To whom correspondence should be addressed.
E-mail: jianghwwh@163.com

this harmful process would cause agglomeration of an entire fluidized bed and consequent defluidization [4-8]. Therefore, prevention and diagnosis of agglomeration are important to avoid unplanned shutdown and expensive maintenance interruption for fluidized bed boilers. Once particle agglomeration happens, it will strongly disturb the pressure distribution inside a fluidized bed. Coal combustion under reducing condition is probably accompanied by agglomeration, and undergoes great pressure fluctuations [9]. During biomass combustion, within a time interval before agglomeration, an unstable pressure distribution was observed, and the variance of pressure variation showed a decreasing trend in the agglomeration process [10]. For the above connection between agglomeration phenomenon and pressure variation in fluidized beds, the method of using pressure fluctuation signal analysis to detect the occurrence of agglomeration inside fluidized beds has recently attracted wide concern from investigators.

However, in actual operations of CFB boilers, due to the exposure to the gas-solid flow, pressure measuring points fixed inside furnaces, which were reported from most papers [11-15], the problem of frequent blockages existed and were easy to be worse. These may reduce the reliability of monitoring results. As fluidizing air flows through a wind cap, the pressure fluctuations of airflow inside the wind cap inlet are closely related to the pressure fluctuations of gas-solid flow near the wind cap outlet in the furnace [16]. If the pressure measuring points are mounted on the entrance walls of wind caps under the distribution plate, owing to being out of touch with solids in furnace, the damage to measuring points, due to the washing of solids, can be avoided. The reliability of condition monitoring of gas-solid flow can be thereby improved.

In this paper, by means of a cold CFB system, partial blockages of the wind cap near the bed wall of feeding side, partial blockages of the wind cap near the bed wall of recycling side, as well as agglomeration of different extents inside the bed, were simulated. During the process of fault simulation, pressure fluctuation signals of measuring points fixed at the inlets of wind caps were measured under the stable operation condition of different primary air velocities. The signals were then analyzed with the methods of statistical average, standard deviation, wavelet analysis and homogeneous index calculation. After calculations, relevant characteristic parameters of signals were obtained. Based on the variations of these parameters, characteristics of pressure fluctuations in wind caps and characteristics of gas-solid fluidization in the bed, which accompanied partial blockages of two wind caps or agglomeration of different extents inside the bed, were analyzed.

EXPERIMENTAL APPARATUS AND METHODS

A cold CFB apparatus, sketched in Fig. 1, was used to simulate faults of wind cap partial blockages and agglomeration in the bed. During the process of simulating a fault, pressure fluctuation signals were measured, which came from the pressure taps fixed on the inlets of several wind caps of different cross-sectional positions. The cross-sectional dimensions of the riser were 0.288 m in length, 0.288 m in width and 4 m in height. Wind caps of bell-type were mounted on the distribution plate with five rows and five columns.

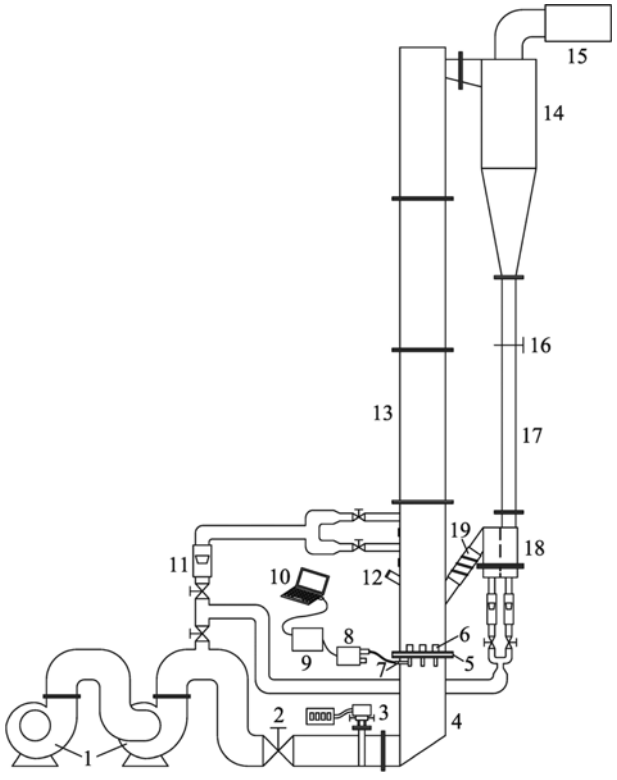

Fig. 1. Schematic diagram of experimental apparatus.

1. Centrifugal fan	10. Computer
2. Control valve	11. Rotameter
3. Uniform velocity tube flow meter	12. Feed inlet
	13. Riser
4. Air chamber	14. Cyclone
5. Distribution plate	15. Bag filter
6. Wind cap	16. Butterfly valve
7. Pressure tap	17. Standpipe
8. Differential pressure sensor	18. Loop seal
9. Data acquisition module	19. Recirculation pipe

Based on the numerical value of primary air volume displayed on the uniform velocity tube flow meter of ANB-200 type, the velocity of primary air could be regulated with a valve. The measuring range of the flow meter was in the range of 400-2,000 m^3/h, with the flow uncertainty of 2.00%. The flow uncertainty C_{qv} was estimated by the formula below:

$$C_{qv}=\pm\left(\frac{\sigma Q_v}{Q_v}\right)=\pm 2\left[\left(\frac{\sigma\varphi}{\varphi}\right)^2+4\left(\frac{\sigma D}{D}\right)^2+\frac{1}{4}\left(\frac{\sigma\Delta p}{\Delta p}\right)^2+\frac{1}{4}\left(\frac{\sigma\rho}{\rho}\right)^2\right] \quad (1)$$

where Q_v, φ, D, Δp, ρ, respectively, denote volume flow rate, correction coefficient of flow rate, inside diameter of the pipe, difference between total pressure and static pressure of fluid, and fluid density, while σQ_v, $\sigma\varphi$, σD, $\sigma\Delta p$, σ, ρ respectively, represent absolute errors of Q_v, φ, D, Δp and ρ. The calculation formula of volume flow rate Q_v was:

$$Q_v=\varphi D^2\sqrt{\Delta p/\rho} \quad (2)$$

Theoretical principle of the flow meter is based on the equal area distribution method, as well as the description of flow velocity distribution equation using multiple measuring points and approxi-

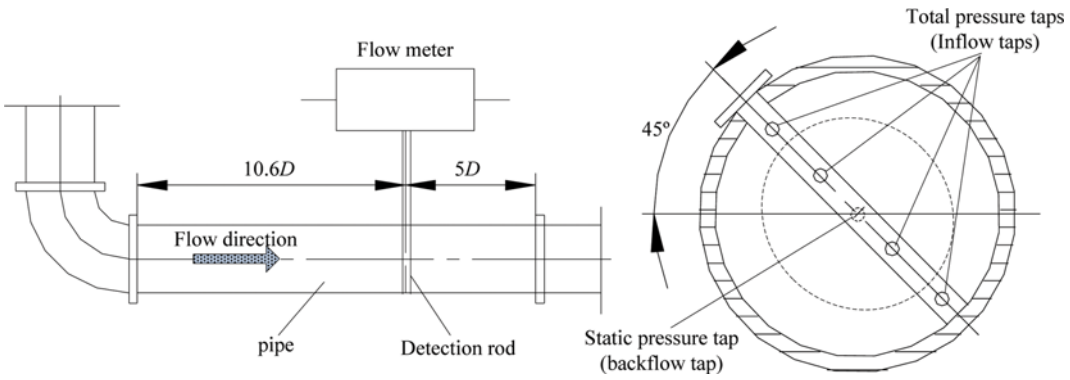

Fig. 2. Installation diagram of uniform velocity tube flow meter.

mate integration theory. To obtain the flow velocity distribution of fully developed pipe flow, for a high measurement accuracy, a straight pipe of length 10.6D was connected before the flow meter, and a straight pipe of length 5D was connected behind. Detection rod of the flow meter was fixed in pipeline diameter direction, with an upward tilt of 45 degrees for a higher-accuracy aerometry. Installation diagram of uniform velocity tube flow meter in pipeline is shown in Fig. 2.

Measurement equipment used to acquire pressure signals included differential pressure sensors of type CGYL-300b, one multifunction data acquisition module of type USB7360 and one computer. Differential pressure sensors were used to measure the pressure signals in the range of zero to fifteen kilopascal, whose response time did not exceed one millisecond. In the signal acquisition process, a sampling frequency of 100 Hz was chosen, and 16384 data of each set were acquired.

To prevent fan surge impacting the stability of air flow in the system, which often occurs when the flow rate is too small, only one fan was used to provide fluidization gas under the condition of lower primary air velocity, while two series-wound fans were used to provide fluidization gas under the condition of higher primary air velocity. A vertical dotted line was used to make a distinction between the operating condition of single fan and two series-wound fans in Fig. 6-10, the lateral axis variable of which represented primary air velocity. When measured data were compared, data of the same fan operating condition were used.

Before simulating partial blockages of the wind caps, the distribution plate was discharged from the cold CFB. Looking down on the upper surface of the distribution plate, based on its mounting direction, adhesive tape was used to seal up four orifices of the wind cap located at the central position of the leftmost column (feeding side); then they were used to seal up four orifices of the wind cap located at the central position of the rightmost column (recycling side). Based on the operation of this treated distribution plate, partial blockage of the wind cap near the bed wall of feeding side, together with partial blockage of the wind cap near the bed wall of recycling side, were simulated. Blocked positions are shown in Fig. 3. Blocked position 1 corresponded to four orifices near the left bed wall of wind cap C2 shown in Fig. 4, while blocked position 2 corresponded to four orifices near the right bed wall of wind cap C3 shown in Fig. 4. After the finish of sealing up

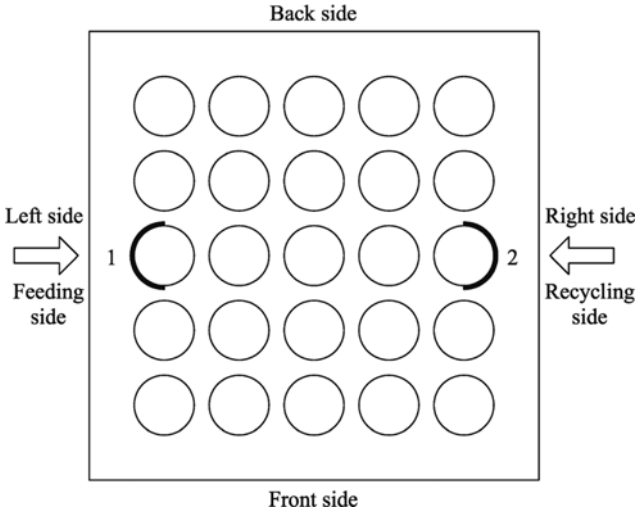

Fig. 3. Mimic diagram of wind cap partial blockages.

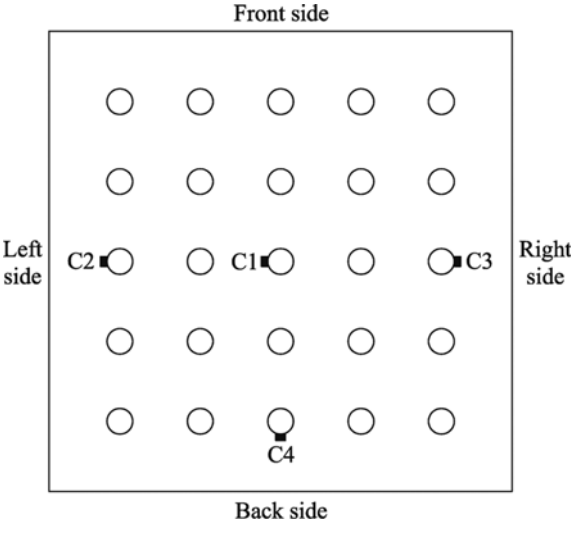

Fig. 4. Schematic diagram of pressure measuring points fixed on the inlets of wind caps.

orifices of two wind caps, a distribution plate was installed back to the cold CFB; then wide size range particles of 40 kg weight were

Table 1. Procedures of simulating agglomeration in the CFB

Sequence	Mass of feeding agglomerate particles M_{fap} (kg)	Sizes of feeding agglomerate particles d_{fap} (μm)	Agglomeration extent of the bed δ (%)	Sizes of agglomeration in the bed after feeding d_{bap} (μm)
1	0.2	1400-1700	0.5	1400-1700
2	0.5	1400-1700	1.7	1400-1700
3	0.8	1400-1700	3.7	1400-1700
4	0.7	1700-2360	5.4	1400-2360
5	0.8	1700-2360	7.3	1400-2360
6	1.0	2360-4750	9.6	1400-4750

put as bed materials into the bed, whose mean particle diameter was 562 μm and particle true density was 2,600 kg/m^3. After the finish of the aforementioned work, fans were turned on; then volumes of primary air and loop seal air were regulated to make the CFB operating stably. During the stable operation condition of different primary air velocities, pressure signals measured from blocked wind caps C2 and C3, as well as signals measured from unblocked wind cap C4, were acquired.

In the process of simulating agglomeration, wide size range particles of 40 kg weight were also used as initial bed materials, whose particle size distribution were the same as initial bed materials used in simulating partial blockages of the wind caps. Coarse particles of different particle sizes and different masses, whose sizes were larger than initial bed materials, were used as agglomeration particles of different extents. Before simulating agglomeration phenomena of certain extent, a certain mass of initial bed materials was taken out from the bed; then agglomeration particles of the same mass were added to the bed to keep the total mass of the bed materials unchanged. Under a stable operation condition of certain primary air velocity, along with a certain extent of agglomeration, pressure fluctuations in the central wind cap were measured. After the signal measurement of the previous condition, primary air velocity was reduced to a small numerical value to make the bed be fluidized in bubbling fluidization. Experimental procedures were repeated to simulate a severer extent of agglomeration, and to measure pressure fluctuations in the wind cap under agglomeration of this extent.

The mathematical definition for agglomeration extent δ of the bed is:

$$\delta = 100 \times \sum_{m=1}^{3} M_{apm,n}/M_{bed},\ m=1, 2, \ldots, 3,\ n=1, 2, \ldots, 6. \quad (3)$$

$$M_{apm,n} = M_{apm,n-1} - 0.01 M_{fapm,n} \times R_{apm,n-1} + M_{fapm,n} \quad (4)$$

$$R_{apm,n-1} = 100 \times M_{apm,n-1}/M_{bed} \quad (5)$$

where $M_{apm,n}$ represents the mass of agglomerate particles of label number m in the bed, while m=1 denotes particle size distribution of 1,400-1,700 μm; m=2 denotes particle size distribution of 1,700-2,360 μm; m=3 denotes particle size distribution of 2,360-4,750 μm; and n denotes the sequence of simulating agglomeration. In the formulas, M_{bed} is the mass of total bed particles, while $M_{fapm,n}$ and $R_{apm,n-1}$ are, respectively, the mass of feeding agglomerate particles of label number m in the sequence n and the weight percent of agglomerate particles of label number m in the bed after feeding agglomerate particles in sequence n−1.

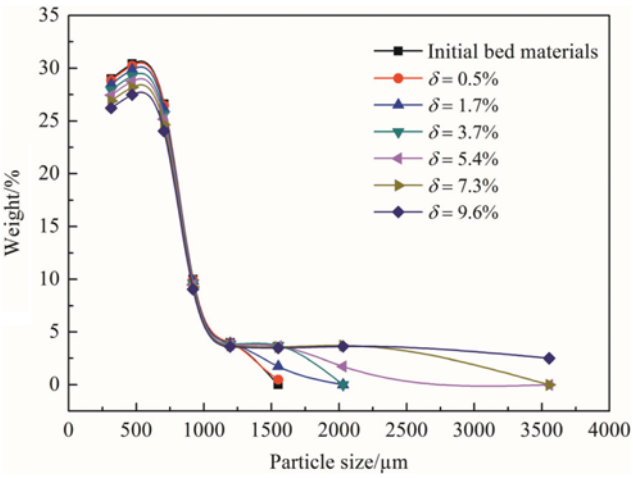

Fig. 5. Particle size distributions of initial bed materials and agglomerate bed materials of different δ.

Table 1 shows the detailed procedures of simulating agglomeration in the bed. In Table1, particle size range and mass of feeding coarse quartz sand particles at each turn are listed, as well as the agglomeration extent and sizes of agglomeration in the bed, after feeding agglomerate particles in each sequence. Particle size distributions of initial bed materials and agglomerate bed materials of different δ are shown in Fig. 5.

ANALYSIS METHOD

1. Signal Preprocessing

To study the amplitude-frequency characteristics of pressure fluctuations, before signals were analyzed, the mean values were removed from the initial measured signals. Based on these previous treated signals, amplitude-frequency characteristics of pressure fluctuations were analyzed with several mathematical techniques, such as statistical average, standard deviation, wavelet analysis and homogeneous index calculation.

2. Statistical Standard Deviation

The mathematical definition for the standard deviation of pressure fluctuation signals p_i is:

$$\sigma = \sqrt{\frac{1}{I-1}\sum_{i=1}^{I}(p_i - \bar{p})^2},\ i=1, 2, 3, \ldots, I \quad (6)$$

In the formula, the pressure average value should be expressed as:

$$\overline{p}=\frac{1}{I}\sum_{i=1}^{I}p_i \tag{7}$$

3. Wavelet Analysis

Wavelet analysis, which is an effective technique to identify gas-solid flow characteristics of fluidized beds [17-19], is used to represent or approach one signal with a series of functions. Wavelet transform of a continuous signal x(t) is defined as:

$$W_f(a,b)=\frac{1}{\sqrt{|a|}}\int_{-\infty}^{+\infty}x(t)\,\psi^*\left(\frac{t-b}{a}\right)dt \tag{8}$$

where $W_f(a, b)$ denotes a wavelet coefficient, while $\psi^*(t)$ represents a basic wavelet function. In the formula, a and b are, respectively, a dilation factor and a translation factor, whose values range from $-\infty$ to ∞ with $a\neq 0$.

A wavelet function is a series of high-frequency and finite-length sequences transformed from a basic wavelet function with dilation and translation:

$$\psi(t)=\frac{1}{\sqrt{|a|}}\psi^*\left(\frac{t-b}{a}\right) \tag{9}$$

The objective of transform is to realize a gradual approximation to a signal with different resolutions. Therefore, wavelet analysis has features of time-frequency localization and multi-resolution for signals.

An initial signal is decomposed into its approximation and detail parts of different frequency bands by wavelet transform. The decomposition process is carried on continuously until the desired level J is reached. A continuous signal $x(t_i)$ can be approximately expressed by orthogonal wavelet series as:

$$x(t_i)\approx A_j(t_i)+D_j(t_i)+D_{j-1}(t_i)+\cdots+D_1(t_i) \tag{10}$$

where $D_1(t_i)$, $D_2(t_i)$, $\cdots$, $D_j(t_i)$ represent detail signals at resolutions 2^j, and $A_j(t_i)$ denotes the approximation signal at resolution 2^j.

In this paper, pressure fluctuation signals were decomposed by wavelet analysis technique with Daubechies (dbN) wavelet until the decomposition level seven was reached. There is not a specific expression for dbN wavelet function, except for N=1. But its modulus square of transition function h is specific and has the following relationship:

$$|m_0(\omega)|^2=\left(\cos^2\frac{\omega}{2}\right)^N\sum_{k=0}^{N-1}C_k^{N-1+k}\left(\sin^2\frac{\omega}{2}\right)^k \tag{11}$$

In the formula,

$$m_0(\omega)=\frac{1}{\sqrt{2}}\sum_{k=0}^{N-1}h_k e^{-jk\omega} \tag{12}$$

where N denotes the order of Daubechies wavelet, C_k^{N-1+k} represents binomial coefficient, ω represents angular frequency. Effective support width of dbN wavelet function is $2N-1$. In consideration of having enough amount of data of each set, and for a shorter computation time and producing fewer wavelet coefficients of high amplitude [20,21], which will both satisfy the needs of engineering calculation and signal feature extraction, Daubechies wavelet of the second order (N=2) was chosen as an optimized wavelet.

Sampling frequency of 100 Hz was used, whose detection range was 0-50 Hz. According to the principle of wavelet transform, the corresponding frequency band of sub-signal D_1 was 25-50 Hz, D_2 was 12.5-25 Hz, D_3 was 6.25-12.5 Hz, D_4 was 3.125-6.25 Hz, D_5 was 1.563-3.125 Hz, D_6 was 0.781-1.563 Hz, and D_7 was 0.391-0.781 Hz.

The squared sum of amplitude was defined as the energy of a signal:

$$E=\sum_{i=1}^{I}|x(t_i)|^2 \tag{13}$$

Simultaneously, E_j^D and E_J^A were, respectively, defined as the cumulative energy of detail signals at different level j and approximation signal at level J.

$$E_j^D=\sum_{i=1}^{I}|D_j(t_i)|^2,\ i=1, 2, \ldots, I,\ j=1, 2, \ldots, J \tag{14}$$

$$E_J^A=\sum_{i=1}^{I}|A_J(t_i)|^2 \tag{15}$$

4. Homogeneous Index

Pressure fluctuation signals were analyzed with wavelet multi-resolution analysis as introduced in formula (8)-(10), until the decomposition level seven was reached. After the analysis, eight subsignals, D_1, D_2, D_3, D_4, D_5, D_6, D_7 and A_7, were acquired, whose relevant frequency bands were listed from high frequency to low frequency. These subsignals were divided to three specific scales, which were the micro-scale related to higher frequency and small fluctuations (S_{SF}), meso-scale related to intermediate frequency and large fluctuations (S_{LF}), and macro-scale related to lower frequency (S_{DC}).

Micro-scale subsignals S_{SF} are defined as follows:

$$S_{SF}=\sum_{j=1}^{q}D_j(t),\ 1\le q<J \tag{16}$$

The subsignals represented the sum of detail signals below level q and had an approximate frequency bands of $[f_s/2^{q+1}, f_s/2]$ Hz, where f_s is the sampling frequency. It mainly captured the information of particle movement, small and rapid bubbles or voids. Meso-scale subsignals S_{LF} are defined as

$$S_{LF}=\sum_{j=q+1}^{J}D_j(t),\ 1\le q<J \tag{17}$$

where the maximum decomposition level J was set as seven. The approximate frequency bands of subsignals S_{LF} were from $f_s/2^{J+1}$ Hz to $f_s/2^{q+1}$ Hz, which denoted the fluctuation information of large bubbles or voids. Macro-scale subsignals S_{DC} were equal to $A_J(t)$, whose frequency band were $[0, f_s/2^{J+1}]$ Hz. They represented the intensity of moving average in the initial treated signals.

As the primary air velocity was regulated, the gas-solid flow condition in the bed was changed, a competition would be brought between the energy of S_{SF} and S_{LF}. Based on this mechanism, a variable called homogeneous index H was defined, which was determined by the proportion of the energy of S_{SF} and S_{LF} [22]. The variable could characterize the transition of gas-solid flow conditions. Its definition is shown in a formula as follows:

$$H = \frac{E_{SF}}{E_{LF}} = \frac{\Sigma_{j=1}^{q} D_j^2(t)}{\Sigma_{j=q+1}^{J} D_j^2(t)} \quad (18)$$

In the formula, E_{SF} represents the energy of micro-scale subsignal S_{SF}, its unit is the square of kilopascal, while E_{LF} represents the energy of meso-scale subsignal S_{LF}, its unit is the same as E_{SF}.

Obviously, the larger E_{SF} is relative to E_{LF}, the larger the contribution of particle motions, inter-particle collisions and small bubbles or voids to the fluctuations, and more homogeneous gas-solid flow and mixture in the bed. In this paper, for the calculations of homogeneous indices H of signals, the dividing level q between S_{SF} and S_{LF} subsignals was set as three.

RESULTS AND DISCUSSION ON WIND CAP PARTIAL BLOCKAGES

1. Average Values of Pressure Fluctuations in Wind Caps

Fig. 6 reports the relationship between average values p_{ca2}, p_{ca3}, p_{ca4} of pressure fluctuations measured from wind caps C2, C3, C4 and primary air velocity u, under the operation conditions of non-blockage or partial blockages of wind caps C2, C3. Under the normal operation of non-blockage, average values of pressure fluctuations measured from C3, which was near the right bed wall, and pressure fluctuations measured from C4, which was near the back bed wall, were both larger and close to each other. Different from these two parameters, average values of pressure fluctuations measured from C2, which was near the left bed wall, were smaller. These characteristics showed that the bed resistances of areas near the right bed wall and the back bed wall, were larger than that of the area near the left bed wall, under normal operation condition. The reason for these characteristics may be the left bed wall was the incoming flow side, what made the air velocities of outlets of the wind cap near the left bed wall larger than others. This also made the particle concentration of the area near the left bed wall and the bed resistance of this area relatively lower. At higher primary air velocities, the spaces over wind cap C3 and wind cap C4, which were respectively near the right wall and the back wall, were influenced by recycling particles that particle concentrations of these spaces were higher than other spaces. This may be the reason for larger values of p_{ca3} and p_{ca4}.

When the wind cap C2 and wind cap C3 were partially blocked, flow areas of through holes of these two wind caps decreased. As a result, pressure drops of air flowing through wind cap C2 and wind cap C3 both had an obvious increase, which made p_{ca2} and p_{ca3} obviously larger than p_{ca4}. It was further observed from Fig. 6 that, under operations of wind cap partial blockages, the slopes of the relationships between average values of pressure fluctuations and primary air velocities obviously increased, after the fan operation condition transformed from single fan to two series-wound fans. This phenomenon showed that average values of pressure fluctuations measured from wind caps were more sensitive to the transform of fan operation condition, when the bed was operated under partial blockages of wind caps.

2. Standard Deviation of Pressure Fluctuations in Wind Caps

Fig. 7 shows the relationship between standard deviations σ_{c2}, σ_{c3}, σ_{c4} of pressure fluctuations measured from wind caps C2, C3, C4 and primary air velocity u, under the operation conditions of non-blockage or partial blockages of wind caps C2, C3. The influences of partial blockages of wind caps C2 and C3 on standard deviations σ_{c2}, σ_{c3}, σ_{c4} of pressure fluctuations, which were observed from Fig. 7, were not obvious under lower primary air velocities. However, as the bed was operated under higher primary air velocities, partial blockages of wind caps C2 made σ_{c2} become the minimum one of three values from the maximum one of three values. Partial blockages of wind caps C3 also made σ_{c3} slightly smaller than σ_{c4} in most of the cases under higher air velocities, which originally slightly larger than σ_{c4}. This phenomenon showed that partial blockages of wind caps had a restriction to the gas-solid flow and pressure fluctuations in the spaces over the wind caps. Fig. 7 also showed that standard deviations of pressure fluctuations measured from wind caps were more sensitive to the transform of fan operation condition, when the bed was operated under partial

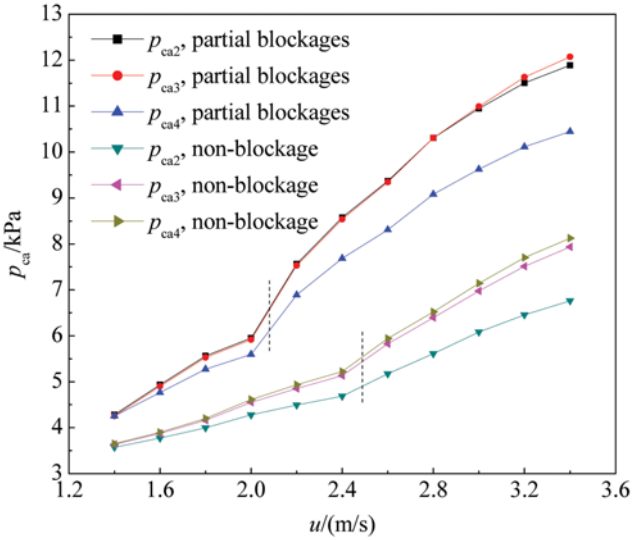

Fig. 6. Effects of wind cap partial blockages on average values of pressure fluctuations.

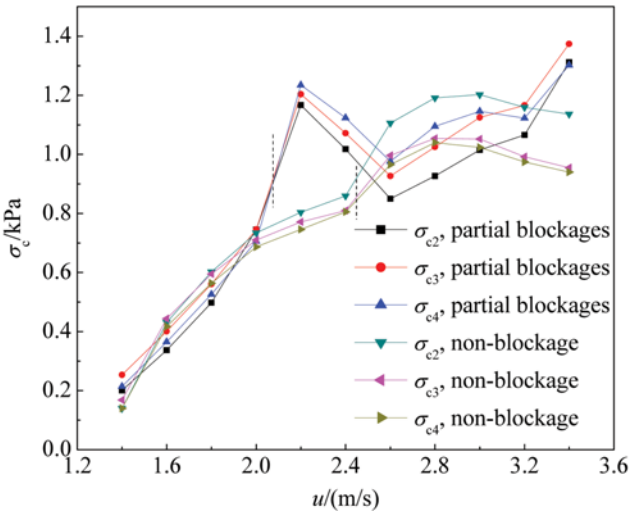

Fig. 7. Effects of wind cap partial blockages on standard deviations of pressure fluctuations.

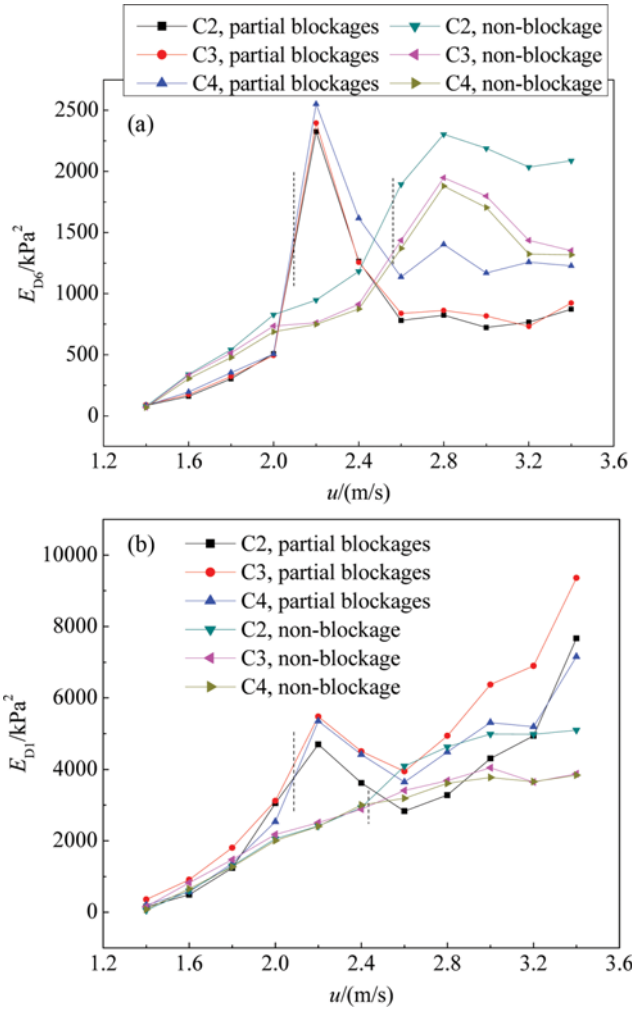

Fig. 8. Effects of wind cap partial blockages on wavelet energy of pressure fluctuations.
(a) Effects of wind cap partial blockages on wavelet energy E_{D6},
(b) Effects of wind cap partial blockages on wavelet energy E_{D1}

blockages of wind caps.

3. Wavelet Energy of Pressure Fluctuations in Wind Caps

Fig. 8 reports the relationship between low-frequency wavelet energy E_{D6}, high-frequency wavelet energy E_{D1} of pressure fluctuations measured from wind caps C2, C3, C4 and primary air velocity u, under the operation conditions of non-blockage or partial blockages of wind caps C2, C3. As shown in Fig. 8(a), under the normal operation of non-blockage, low-frequency wavelet energy E_{D6} of pressure fluctuations detected from wind cap C2, was obviously larger than those of pressure fluctuations detected from wind cap C3 and wind cap C4, but E_{D6} of pressure fluctuations detected from wind cap C4 had a slightly larger than that of pressure fluctuations detected from wind cap C3 in comparison. Under the partial blockages of wind caps C2 and C3, at lower primary air velocities, E_{D6} of pressure fluctuations measured from these three wind caps near the bed wall, were all less than that of normal operation. This phenomenon was due to the reductions of air flow velocities in the bottom bed nearby the bed wall, which was caused by the blockages of wind caps. It made sizes of bubbles and amplitudes of low-frequency pressure fluctuations reduced, in the bottom bed near the bed wall. At higher primary air velocities, E_{D6} of pressure fluctuations measured from these three wind caps near the bed wall, were still less than that of normal operation, but E_{D6} of pressure fluctuations measured from wind cap C4 was larger than those measured from wind caps C2 and C3. The reason is that velocities of air flow in the bottom bed near outlets of wind cap C4 were larger than those near outlets of blocked wind caps C2 and C3, due to the non-blockage of wind cap C4, resulting in sizes of bubbles and amplitudes of low-frequency pressure fluctuations near outlets of wind cap C4 were larger. Besides these, observed from Fig. 8(a), low-frequency wavelet energy E_{D6} of pressure fluctuations measured from wind caps was sensitive and acutely disturbed by the transform of fan operation condition, when the bed was operated under partial blockages of wind caps.

As shown in Fig. 8(b), there were not obvious influences of partial blockages of wind caps on high-frequency wavelet energy E_{D1}, at lower primary air velocities. But at higher primary air velocities, partial blockages of wind caps C3 made E_{D1} of wind cap C3 become to the maximum one of three values from the minor one of three values. This is because of the decreased air velocities near the outlets of wind cap C3, due to the partial blockages of wind caps C3, which resulted in a larger mass of recycling particles falling over wind cap C3 and a larger mass of particles falling along the bed wall. These phenomena caused an increased particle concentration in this space and more frequent inter-particle collisions, which made high-frequency wavelet energy E_{D1} of wind cap C3 increase. Partial blockages of wind caps C2 also made air velocities near the outlets of wind cap C2 decreased, which also resulted in a larger mass of particles falling along the bed wall. But different from wind cap C3, because wind cap C2 was close to incoming flow, its decreased air flow velocities of outlets also made high-frequency fluctuations caused by rising carried particles of bubble

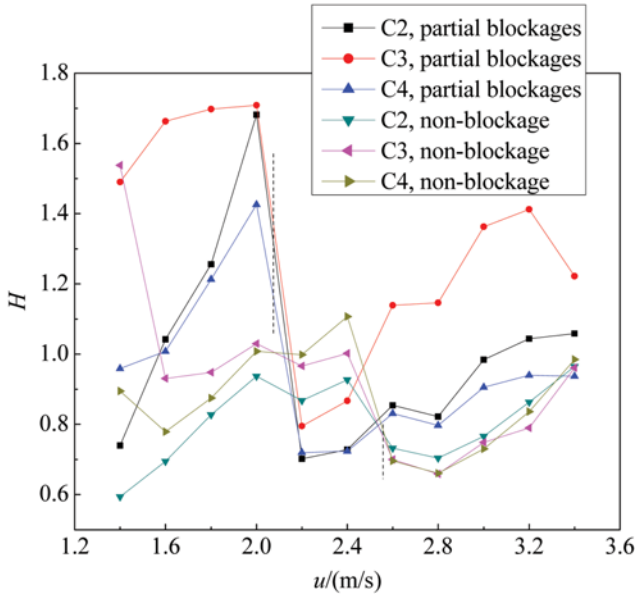

Fig. 9. Effects of wind cap partial blockages on homogeneous indices of pressure fluctuations.

wakes attenuated. These two influences made wavelet energy E_{D1} of wind cap C2 have a lesser difference. Similar to aforementioned signal parameters, high-frequency wavelet energy E_{D1} of pressure fluctuations were also sensitive to the transform of fan operation condition, under the operation with partial blockages of wind caps.

4. Homogeneous Indices of Pressure Fluctuations in Wind Caps

Fig. 9 shows the relationship between homogeneous indices H of pressure fluctuations measured from wind caps C2, C3, C4 and primary air velocity u, under the operation conditions of non-blockage or partial blockages of wind caps C2, C3. Observed from Fig. 9, partial blockages of wind caps C3 made homogeneous index of pressure fluctuations of wind cap C3 increased at most of primary air velocities. The reason is that wind cap partial blockages led to air flow velocities of wind cap outlets be reduced. As a result, sizes of bubbles in this space decreased, simultaneously, recycling particles falling over wind cap C3 and particles falling along the bed wall both grew in number or quantity. These brought about an increased particle concentration in this space and more frequent inter-particle collisions, ratios of high-frequency energy to low-frequency energy of pressure fluctuations thereby increased. Partial blockages of wind cap C2 also led to air flow velocities of outlets of wind cap C2 be reduced. As a result, sizes of bubbles in this space decreased, simultaneously, the number and mass of particles falling along the bed wall increased; eventually ratios of high-frequency energy to low-frequency energy of pressure fluctuations increased. As shown in Fig. 9, homogeneous indices H of pressure fluctuations under partial blockages of wind caps were acutely disturbed and more sensitive by the transform of fan operation condition, which confirmed the sensitivity of H to the transform of fan operation condition, during the operation under partial blockages of wind caps.

RESULTS AND DISCUSSION ON AGGLOMERATION

The fluidized bed with simulating agglomeration faults of different extents was operated at the stable conditions of primary air velocity 2 m/s or 3 m/s. In view of the relationship between standard deviations of pressure fluctuations measured from wind caps C1, C2, C3, C4 and fluidization gas velocities (shown in Fig. 10), which was acquired from the bed only with initial bed materials, standard deviations of pressure fluctuations increased with increasing fluidization gas velocity around 2 m/s, while they decreased or fluctuated in a certain range with increasing fluidization gas velocity around 3 m/s. Based on fluidization theory, sizes of bubbles and amplitudes of fluctuations increase with increasing fluidization gas velocity in bubbling fluidized beds, but they will be reduced or restricted in turbulent fluidization. Thus, it can be judged that the bed was fluidized in bubbling fluidization around fluidization gas velocity 2 m/s, but around fluidization gas velocity 3 m/s, its dense-phase bed was fluidized in turbulent fluidization. Besides these, under the stable conditions of gas velocity 3 m/s, dilute phase pneumatic conveying of small particles was observed from the top of the bed, and a small quantity of recycling particles were watched from the standpipe.

1. Average Values of Pressure Fluctuations in Wind Caps

Fig. 11 reports average values p_{ca} of pressure fluctuations measured from wind caps C1, C2, C3, C4, under simulating agglomeration of different extents δ, at the stable conditions of primary air velocity 2 m/s or 3 m/s. In Fig. 11, average pressures p_{ca} inside wind caps C1, C2, C3, C4 all increased with increasing agglomeration extent, under the stable conditions of two gas velocities. This is because as agglomeration extent increased, fluidization performance of the bed became worse, and bed resistance against air flow grew larger, average pressures p_{ca} of air flow in inlets of wind caps thereby increased.

2. Standard Deviations of Pressure Fluctuations in Wind Caps

Fig. 12 shows standard deviations σ_c of pressure fluctuations measured from wind caps C1, C2, C3, C4, under simulating agglomeration of different extents δ, at the stable conditions of primary air velocity 2 m/s or 3 m/s. The figure could reflect the effects of the increase of agglomeration extent on the total pressure fluctuations.

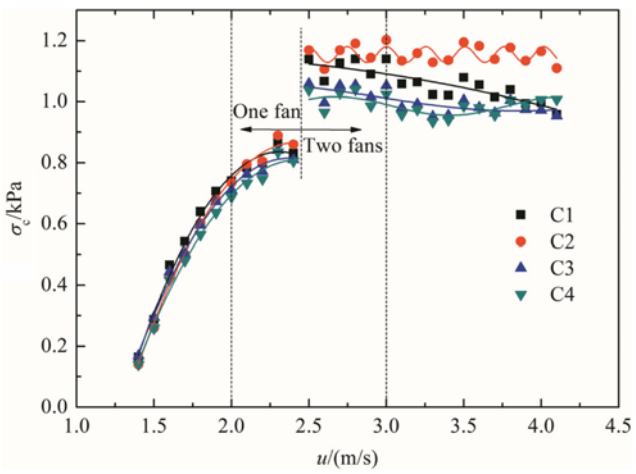

Fig. 10. Standard deviations of pressure fluctuations at different fluidizing velocities using initial bed materials.

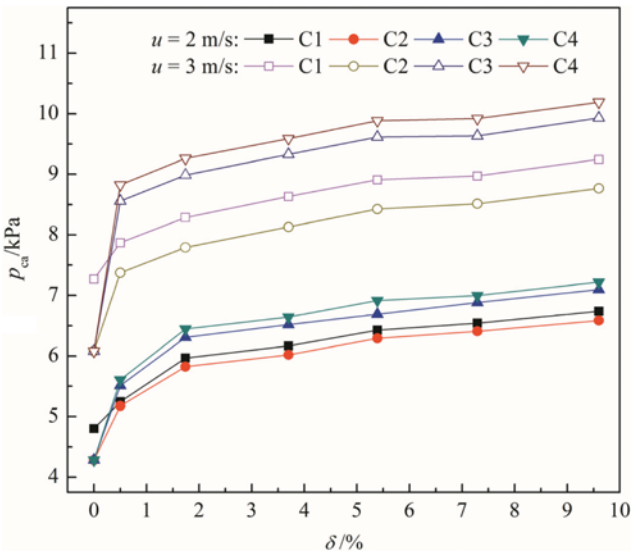

Fig. 11. Effects of agglomeration on average values of pressure fluctuations.

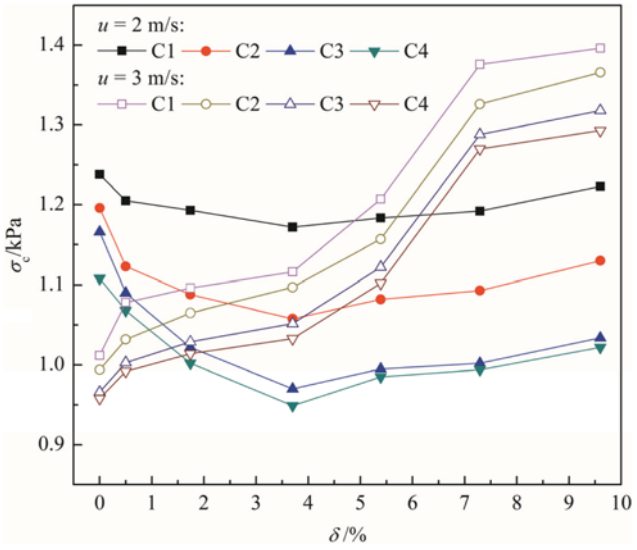

Fig. 12. Effects of agglomeration on standard deviations of pressure fluctuations.

Seen from Fig. 12, under primary air velocity of 2 m/s, standard deviations σ_c of pressure fluctuations decreased with increasing agglomeration extent, in the bed with lower agglomeration extent of δ=0 to 3.7, while they increased with increasing agglomeration extent in the bed with higher agglomeration extent of δ=3.7 to 9.6. This is because in a bubbling fluidized bed of lower agglomeration extent, agglomeration of a larger extent led fluidization performance to be worse, and made bubbling intensity damp, amplitudes of pressure fluctuations thereby decreased. When agglomeration extent of the bubbling fluidized bed continuously increased, Geldart D particles increasing in the bottom of the bed, became fluidized in the form of large and slow bubbles [23], which was a marked feature of the fluidization of Geldart D particles. This fluidization feature made standard deviations σ_c of pressure fluctuations increase.

Fig. 13(a) shows fluidization regimes under agglomeration simulations of δ=0 to 9.6, at u=2 m/s. Seen from the figure, bed expansion reduced under the increase of agglomeration extent, while sizes of bubbles in the bottom of the bed came to increase during the process. It can be observed from the last three subfigures that large bubbles were produced in the dense phase. These phenomena seen from the fluidization regimes under agglomeration simulations of different δ at u=2 m/s, can well justify our analysis.

Different from gas velocity of 2 m/s, under primary air velocity of 3 m/s, standard deviations σ_c of pressure fluctuations increased with increasing agglomeration extent from δ=0 to δ=9.6. The reason is that when dense-phase bed was fluidized in turbulent fluidization, the increasing of agglomeration extent had a restriction on the turbulent effects of turbulent fluidization regime, which restricted the growths of bubbles or voids, and amplitudes of pressure fluctuations thus increased. Besides this, large and slow bubbles which were produced in the fluidization of the bottom in-

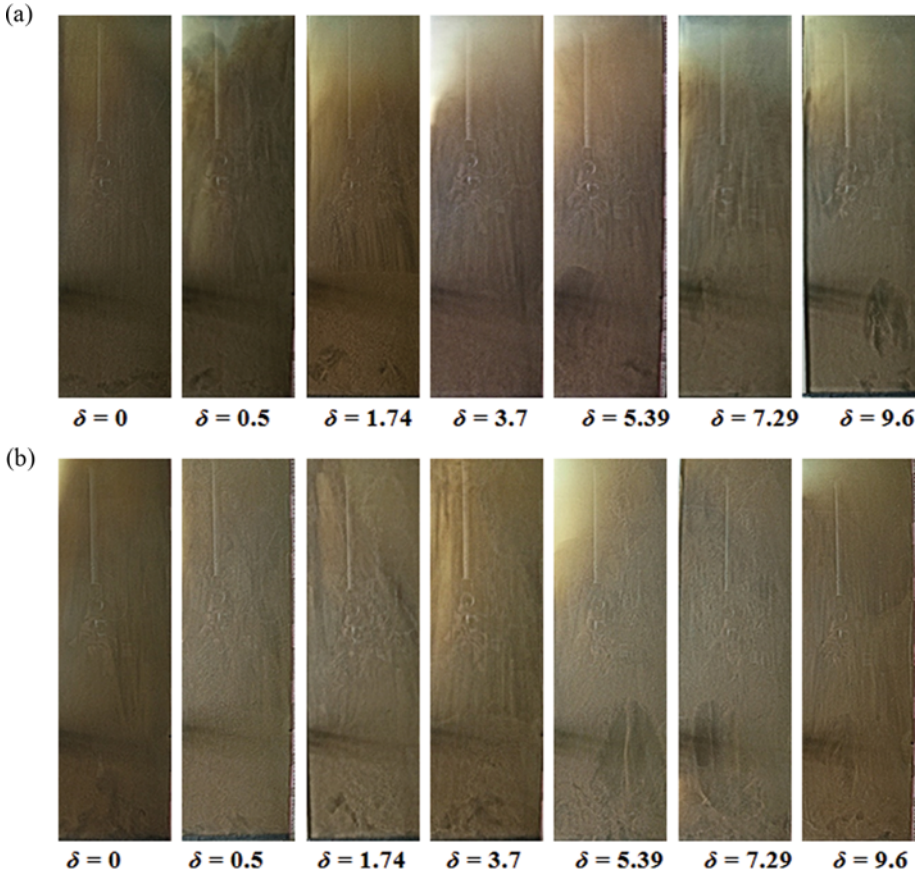

Fig. 13. Fluidization regimes under agglomeration simulations of δ=0 to 9.6, at u=2 m/s or 3 m/s.

creasing Geldart D particles, also made standard deviations σ_c of pressure fluctuations increase. This explanation could be justified by Fig. 13(b), which shows fluidization regimes under agglomeration simulations of δ=0 to 9.6, at u=3 m/s. Large and slow bubbles were very obvious in the subfigures of δ=5.39 to 9.6.

3. Wavelet Energy of Pressure Fluctuations in Wind Caps

Fig. 14 reports wavelet energy E_{D6} and E_{D1} of pressure fluctuations measured from wind caps C1, C2, C3, C4, under simulating agglomeration of different extents δ, at the stable conditions of primary air velocity 2 m/s or 3 m/s. The two subfigures could, respectively, reflect the effects of the increase of agglomeration extent on the low-frequency pressure fluctuations and high-frequency pressure fluctuations.

As shown in Fig. 14(a), under primary air velocity of 2 m/s, low-frequency wavelet energy E_{D6} of pressure fluctuations decreased with increasing agglomeration extent, in the bed with lower agglomeration extent of δ=0 to 3.7, while they increased with increasing agglomeration extent in the bed with higher agglomeration extent of δ=3.7 to 9.6. The reason is like that for σ_c of pressure fluctuations that in the bubbling fluidized bed of δ=0 to 3.7, agglomeration of a larger extent made fluidization performance worse and expansion height of the bed lower, simultaneously made bubble sizes decreased, and energy of low-frequency pressure fluctuations thereby decreased. But as agglomeration extent of the bubbling fluidized bed continuously increased, coarse particles increasing at the bottom were fluidized with large and slow bubbles. They made low-frequency fluctuation energy increase.

At primary air velocity of 3 m/s, low-frequency wavelet energy E_{D6} of pressure fluctuations increased with increasing agglomeration extent from δ=0 to δ=9.6. It is because when the dense-phase bed was fluidized in turbulent fluidization, the increasing of agglomeration extent restricted the turbulent effects, resulting in both the growths of bubbles or voids of Geldart B particles and Geldart D particles, low-frequency fluctuation energy of pressure fluctuations thereby increased.

As shown in Fig. 14(b), high-frequency wavelet energy E_{D1} of pressure fluctuations decreased with increasing agglomeration extent from δ=0 to δ=3.7, as primary air velocity was 2 m/s. This is because rising carried particles of bubble wakes and splashing particles from the bed surface both attenuated due to the decrease of bubble sizes in bubbling fluidization, which was caused by increasing agglomeration extent and worse fluidization performance. In the process of increasing agglomeration extent from δ=3.7 to δ=9.6, E_{D1} of pressure fluctuations gradually increased. The reason is that during this process, the growth of large bubbles caused by the fluidization of increasing Geldart D particles, the reduction of expansion height and increasing particle concentration in dense phase, all made the high-frequency collisions of particles more intense.

As primary air velocity was 3 m/s, high-frequency wavelet energy E_{D1} of pressure fluctuations increased with increasing agglomeration extent. This is because of the increase of inter-particle collisions due to the increase of bubble or void sizes in turbulent fluidiza-

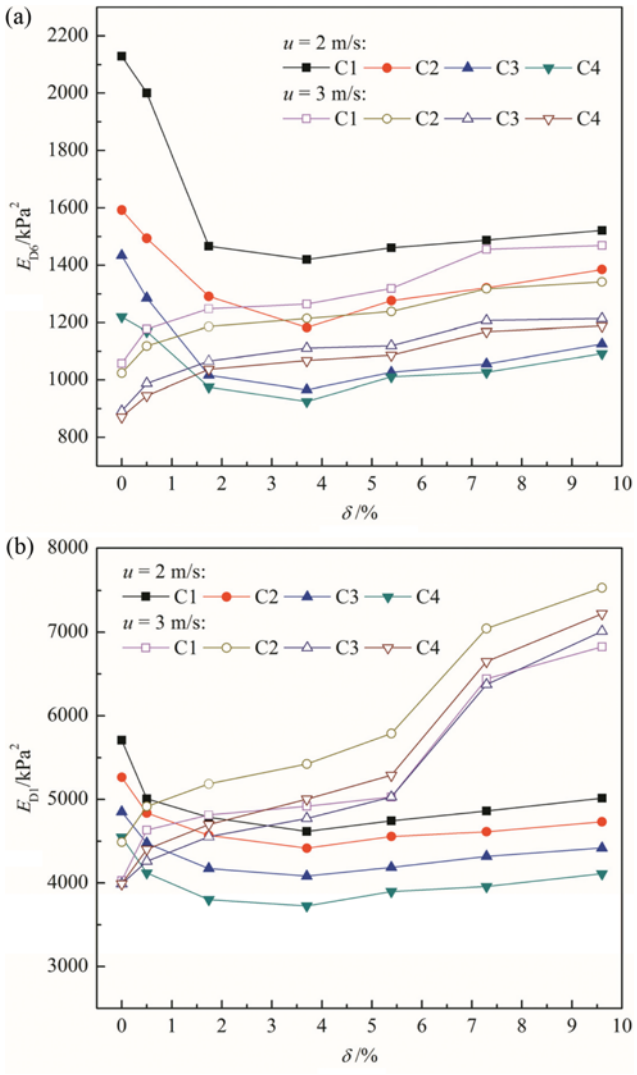

Fig. 14. Effects of agglomeration on wavelet energy of pressure fluctuations.
(a) Effects of agglomeration on wavelet energy E_{D6}. (b) Effects of agglomeration on wavelet energy E_{D1}

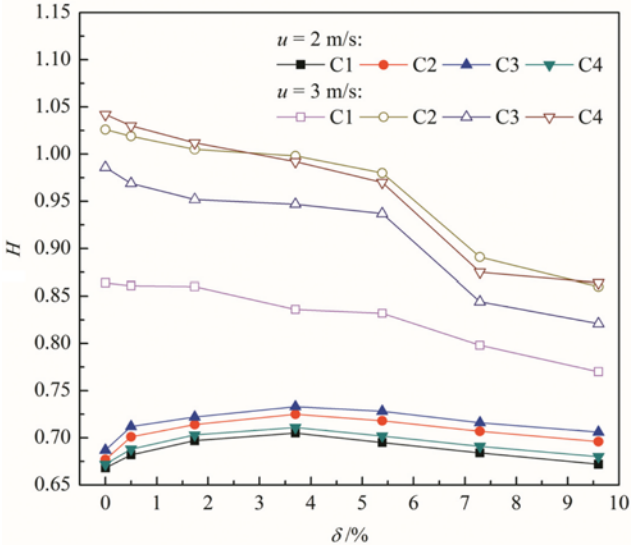

Fig. 15. Effects of agglomeration on homogeneous indices of pressure fluctuations.

tion of dense-phase bed, which was caused by the restriction on the turbulent effects of increasing agglomeration as well as growths of large bubbles of bottom Geldart D particles.

4. Homogeneous Indices of Pressure Fluctuations in Wind Caps

Fig. 15 shows homogeneous indices H of pressure fluctuations measured from wind caps C1, C2, C3, C4, under agglomeration of different extents δ, at stable operation conditions of primary air velocity 2 m/s or 3 m/s. They can reflect the effects of the increase of agglomeration extent on the ratio of high-frequency pressure fluctuation energy to low-frequency pressure fluctuation energy.

As shown in Fig. 15, at primary air velocity of 2 m/s, homogeneous indices H of pressure fluctuations increased with increasing agglomeration extent from δ=0 to δ=3.7. This phenomenon reflected the fluidization characteristic of bubbling fluidization. In bubbling fluidized bed, a more intense bubbling will bring about more inhomogeneous fluctuations in the bed. Agglomeration of a larger extent made bubbling fluidization performance be weakened and sizes of bubbles decreased, but made fluctuations in the bed more homogeneous, so the ratio of high-frequency energy to low-frequency energy thus increased. But in the increasing process of agglomeration extent from δ=3.7 to δ=9.6, homogeneous indices H showed a decreasing trend. In this process, large bubbles of bottom increasing Geldart D particles were produced, which made fluctuations in the whole bed begin to be more inhomogeneous.

Different from the conditions in bubbling fluidization, H of pressure fluctuations decreased with increasing agglomeration extent from δ=0 to δ=9.6, at primary air velocity of 3 m/s. This trend reflected the fluidization characteristic of turbulent fluidization. In a turbulent dense-phase bed, a more intense turbulent fluidization will bring about more homogeneous fluctuations in the bed. A larger agglomeration extent led fluidization performance to be worse and made sizes of bubbles increased, which made fluctuations in the bed trend to inhomogeneous and the proportion of high-frequency energy to low-frequency energy trend to decrease. Besides this phenomenon, it can be noted from Fig. 15 that H of pressure fluctuations measured from wind caps C2, C3, C4, was obviously larger than that of wind caps C1, because of the more dense concentration of particles in the space near the bed walls than the center space.

CONCLUSIONS

The effects of partial blockages of wind caps and agglomeration faults on the fluidization characteristics in a CFB were detected based on the relationship between characteristic parameters of pressure fluctuations measured from wind cap inlets and primary air velocity, as well as the relationship between characteristic parameters of pressure fluctuations and agglomeration extent.

Results of simulating wind cap partial blockages showed that under the operation conditions of wind cap partial blockages, pressure drops of air flowing through blocked wind caps were markedly reduced. Partial blockages of wind caps made low-frequency wavelet energy of pressure fluctuations in blocked wind caps less than that under normal conditions or in other non-blocked wind caps. Partial blockages of the wind cap near the recycling side, resulting in a larger mass of recycling particles falling over the blocked wind cap, as well as a larger mass of particles falling along the bed wall, made high-frequency pressure fluctuation energy in the wind cap increased. Partial blockages of wind caps near the bed walls would make particle concentrations near the bed walls increase and make inter-particle collisions in these spaces become more frequent; thus, homogeneous indices of pressure fluctuations were larger. Characteristic parameters of pressure fluctuations were sensitive or acutely disturbed by the transform of fan operation condition, during the operation under partial blockages of wind caps.

Experimental results of simulating agglomeration showed that average values of pressure fluctuations in wind caps increased with increasing agglomeration extent, in bubbling fluidized bed or dense-phase turbulent bed, because of the worse fluidization performance. In bubbling fluidized bed, increasing agglomeration extent in the range of lower agglomeration extent brought about a worse bubbling fluidization performance and smaller bubble sizes, and made carried particles of bubble wakes and splashing particles from the bed surface both attenuate. As a result, standard deviations, low-frequency and high-frequency wavelet energy of pressure fluctuations all decreased, while homogeneous indices increased. But when agglomeration extent increased in the range of higher agglomeration extent, Geldart D particles increasing in the bottom of the bed, would be fluidized in the form of large and slow bubbles. It made standard deviations, low-frequency and high-frequency wavelet energy of pressure fluctuations all increase, but made homogeneous indices decrease. In dense-phase turbulent bed, increasing of agglomeration extent restricted the turbulent effects, resulting in the growths of bubbles or voids and consequent increase of inter-particle collisions, standard deviations, low-frequency and high-frequency wavelet energy of pressure fluctuations of pressure fluctuations all increased, while homogeneous indices decreased.

ACKNOWLEDGEMENTS

Financial support from National Science & Technology Pillar Program during the Twelfth Five-year Plan Period of China (2012BAA02B01), Specialized Research Fund for the Doctoral Program of Higher Education of China (20090036110008) and General Program, "211 Project" for North China Electric Power University (the 3rd phase) (94021001) are sincerely acknowledged.

NOMENCLATURE

a : dilation parameter
$A_j(t_i)$: approximation signal of multiresolution decomposition at resolution 2^j [Pa]
b : translation parameter
C_{qv} : flow uncertainty
C_k^{N-1+k} : binomial coefficient
d_{bap} : sizes of agglomeration in the bed after feeding [m]
d_{fap} : sizes of feeding agglomerate particles in each sequence [m]
D : inside diameter of the pipe [m]
$D_j(t_i)$: detail signals of multiresolution decomposition at different resolution 2^j [Pa]

E : cumulative energy of a signal [Pa^2]
f_s : sampling frequency [Hz]
H : homogeneous index
i : variable expressing sequence
I : number of samplings
j : variable expressing sequence
J : desired decomposition level of multiresolution decomposition
k : variable expressing sequence
m : label number of agglomerate particles of different particle size distributions
$M_{apm,n}$: mass of agglomerate particles of label number m in the bed after sequence n [kg]
M_{bed} : mass of total bed particles [kg]
$M_{fapm,n}$: mass of feeding agglomerate particles of label number m in the sequence n [kg]
n : sequence of simulating agglomeration
N : order of Daubechies wavelet
$\overline{p}$: average pressure [Pa]
p_{ca} : average value of pressure fluctuations measured in a wind cap [Pa]
p_{cai} : average value of pressure fluctuations measured in wind cap Ci [Pa]
p_i : measured pressure [Pa]
Δp : difference between total pressure and static pressure of fluid [Pa]
q : decomposition level of the boundary between micro-scale and meso-scale subsignals
Q_v : volume flow rate [m^3/s]
$R_{apm,n-1}$: weight percent of agglomerate particles of label number m in the bed after feeding agglomerate particles in sequence n−1
S : pressure signal [Pa]
t : time [s]
u : superficial gas velocity of the primary air [$m \cdot s^{-1}$]
$W_f(a, b)$: wavelet coefficient
x(t) : time sequence function [Pa]

Greek Letters

δ : agglomeration extent of the bed [%]
ρ : fluid density [kg/m^3]
σ : standard deviation [Pa]
φ : correction coefficient of flow rate
$\psi(t)$: wavelet function
$\psi^*(t)$: basic wavelet function
ω : angular frequency [rad/s]

Indices

bap : agglomeration in the bed
bed : total fluidized bed particles
fap : agglomerate particles feeding to the bed
AJ : approximation signal of level J
c : wind cap
ca : average pressure in wind cap
cai : average pressure in wind cap Ci
ci : wind cap symbolized as Ci
DC : low frequency direct current
Dj : detail signals of level j
LF : large fluctuations
s : sampling
SF : small fluctuations

REFERENCES

1. M. Bartels, W. Lin, J. Nijenhuis, F. Kapteijn and J. R. van Ommen, *Progress in Energy and Combustion Science*, **34**, 633 (2008).
2. A. A. Khan, W. de Jong, P. J. Jansens and H. Spliethoff, *Fuel Process. Technol.*, **90**, 21 (2009).
3. R. Chirone, P. Salatino, F. Scala, R. Solimene and M. Urciuolo, *Combustion and Flame*, **155**, 21 (2008).
4. J. Nijenhuis, R. Korbee, J. Lensselink, J. H. A. Kiel and J. R. van Ommen, *Chem. Eng. Sci.*, **62**, 644 (2007).
5. B. Gatternig and J. Karl, *Fuel*, **161**, 157 (2015).
6. J. Silvennoinen and M. Hedman, *Fuel Process. Technol.*, **105**, 11 (2013).
7. P. Chaivatamaset, P. Sricharoon, S. Tia and B. Bilitewski, *Appl. Thermal Eng.*, **50**, 722 (2013).
8. R. Saidur, E. A. Abdelaziz, A. Demirbas, M. S. Hossain and S. Mekhilef, *Renewable and Sustainable Energy Reviews*, **15**, 2262 (2011).
9. P. Selvakumaran and A. K. Bakthavatsalam, *Appl. Thermal Eng.*, **85**, 135 (2015).
10. F. Scala and R. Chirone, *Energy Fuels*, **20**, 120 (2006).
11. C. E. Davies, A. Carroll and R. Flemmer, *Powder Technol.*, **180**, 307 (2008).
12. M. Bartels, J. Nijenhuis, J. Lensselink, M. Siedlecki, W. de Jong, F. Kapteijn and J. R. van Ommen, *Energy Fuels*, **23**, 157 (2009).
13. M. Bartels, J. Nijenhuis, F. Kapteijn and J. R. van Ommen, *Powder Technol.*, **202**, 24 (2010).
14. H. T. Jang, S. B. Kim, W. S. Cha, S. C. Hong and D. S. Doh, *Korean J. Chem. Eng.*, **20**, 138 (2003).
15. S. McDougall, M. Saberian, C. Briens, F. Berruti and E. Chan, *Chem. Eng. Process.*, **44**, 701 (2005).
16. C. Sobrino, N. Ellis and M. de Vega, *Powder Technol.*, **189**, 25 (2009).
17. C. Sheng, Y. Zhao, C. Duan, B. Zhang, P. Feng, K. Lv, W. Yuan, P. Zhang and C. Zhou, *Procedia Eng.*, **102**, 1546 (2015).
18. M. Tahmasebpoor, R. Zarghami, R. Sotudeh-Gharebagh and N. Mostoufi, *Int. J. Multiphase Flow*, **69**, 31 (2015).
19. M. C. Shou and L. P. Leu, *Chem. Eng. Res. Design*, **83**, 478 (2005).
20. I. Daubechies, *Communications on Pure and Applied Mathematics*, **XLI**, 909 (1988).
21. A. Cohen, I. Daubechies and P. Vial, *Appl. Computational Harmonic Analysis*, **1**, 54 (1993).
22. T. Y. Yang and L. P. Leu, *Chem. Eng. Sci.*, **63**, 1950 (2008).
23. A. Svensson, F. Johnsson and B. Leckner, *Int. J. Multiphase Flow*, **22**, 1187 (1996).